Symmetry reduction and control of the dynamics of a 2-D rigid circular cylinder and a point vortex: vortex capture and scattering. *

Banavara N. Shashikanth,
Department of Mechanical Engineering, MSC 3450,
New Mexico State University, Las Cruces,
NM 88003, USA
shashi@nmsu.edu

European Journal of Control, **13** (6), 641–657, 2007.

Abstract

Symmetry reduction and control of the Hamiltonian system of a 2D rigid circular cylinder dynamically interacting with a point vortex external to it is presented. This dynamic model is an idealized example in an inviscid framework of fully-coupled solid-fluid systems interacting in the presence of vorticity and has potential applications to problems in engineering and in nature involving the interaction of coherent vortices with bodies moving (primarily) under their influence. The dynamics of the system generically gives rise to two types of vortex orbits relative to the moving cylinder: bound and scattering orbits. The control input of a bounded external force acting through the cylinder center-of-mass is then added. Exploiting the S^1-symmetry in the system, symplectic reduction is employed to formulate an S^1-invariant control system, that preserves the momentum map, on the two-dimensional symplectic reduced space. On this reduced space, both non-optimal and optimal controllers, the latter using Pontryagin's maximum principle, are investigated with the control objective of changing the vortex orbit from a bound to a scattering type and vice versa.

Keywords: fully-coupled, point vortex, cylinder, optimal control, reduction, scattering

Contents

1 INTRODUCTION

It has become increasingly important in the past few years to gain a better knowledge of the nonlinear fully-coupled dynamics of interacting solid-fluid systems especially for the following applications: the building of energy-efficient small autonomous vehicles (underwater and aerial), an improved understanding of related problems in nature such as fish swimming and bird/insect flight, the study of particle-laden flows and the ever-important topic of vortical structures interacting with moving bodies at high Reynolds numbers, such as aircraft, ships etc. In fact, for *all* these applications one wants to understand the role of coherent vortical structures in the vicinity of the solid body on the motion of the body. The topic of vorticity interacting with solid bodies has of course been well-addressed in the aeronautics literature, especially in the areas of aeroelasticity and vortex-induced oscillations. These previous approaches, however, have typically been either (a) in a linearized framework or (b) in a framework that does not account for the full coupling of the solid and fluid dynamics. Moreover, in most of these approaches the body is held in place or undergoes prescribed motions.

From a dynamics and control point of view it is interesting to first study the problem in a setting in which the body is allowed to move freely under the stress field induced on its boundary by the fluid flow and in which the simultaneous influence of the motion of the body on the fluid is also completely accounted for. Subsequently, constraining or control forces can be imposed on this fully-coupled dynamical model. In particular, a finite-dimensional model to which dynamical systems and control theoretic ideas can be applied would be desirable. With this goal in mind, we study such a finite dimensional model in this paper in which, however, we make the approximation that the

flow is inviscid and, consequently, the stress field on the body is only the pressure field. The dynamics of this model is fully-coupled but only *within* this inviscid framework.

The point vortex model in theoretical fluid mechanics is a popular finite dimensional approximation of a fluid flow with coherent vortical structures [14, 15]. It is a kinetic energy conserving model of the fluid and thus does not account for the dissipative and other effects of viscosity. Hamiltonian point vortex based models of a solid cylinder interacting with vortical structures have been recently constructed by Shashikanth, Marsden, Burdick and Kelly (SMBK) [26, 25] and almost simultaneously by Borisov, Mamaev and Ramodanov (BMR) [22, 4, 3]. In these models a moving 2D rigid cylinder dynamically interacts with N point vortices external to it.

In this paper, the SMBK model is considered for the case of a circular cylinder and when $N = 1$, i.e. there is only one point vortex in the flow. This four-dimensional Hamiltonian system is symmetric under a diagonal action of S^1 and has an associated conserved momentum map. The dynamics of this system is integrable [4]. The motion of the vortex relative to the moving cylinder is typically a bounded orbit or a scattering orbit. The terminology of scattering orbit, borrowed from Eckhardt and Aref [7], refers to orbits that are in the vicinity of the cylinder for a finite period of time but move to infinity, relative to the moving cylinder, for time approaching both positive and negative infinity. This dynamic model is extended to a control model by the addition of a control force acting through the center of mass of the cylinder, see Figure 1. The S^1-symmetry and the Hamiltonian structure of the drift vector field are then exploited to construct an S^1-invariant control system which leaves the momentum map invariant. This control system lies on the two-dimensional symplectic reduced space [13] and is

a planar single-input control system and is thus more amenable to analysis than the original four-dimensional control system.

The control problem investigated on the symplectic reduced space is motivated by a fairly general consideration relevant to all the applications mentioned previously. Namely, there are situations in which the presence of coherent vorticity in the vicinity of the moving body is favorable to the dynamics or motion of the body and there are situations in which it is not. An example of the former would be the transfer of impulse to the body by coherent vortex structures shed in the wake of swimming fish or flying birds [28] and an example of the latter would be the destabilizing effect on the motion of an aircraft or a ship by a strong coherent vortical structure in its vicinity. As a more specific example of the unfavorable effects of vortices, the wake hazard problem which has been a concern for a long time in the aircraft industry [23] should be mentioned. This is the problem of smaller aircraft taking off or landing too closely in the wake of larger aircraft and risking interaction with the trailing vortices shed off the wing tips of the larger aircraft and their consequent destabilizing effects. It is reasonable in such flows to expect scenarios in which the solid body, under the action of a control input, would like to either have a vortex (vortices) in its proximity or break free of it (them). It is of course true that in examples like these the fluid dynamics is more complicated than in our idealized model. Apart from 3D and viscous effects, such as vortex shedding, merging and filamentation, there could also be significant turbulence effects. But, nevertheless, as a start it is interesting to pose, and try to answer the following question in our idealized model: what are the control laws for the force on the circular cylinder to change the vortex orbit from a bound to a scattering type and

vice-versa?

The problem presented in this paper may also be viewed, from a geometric control perspective, as a nice example of utilizing the underlying Hamiltonian structure and symmetries, when they exist, of the drift field to formulate control laws. Indeed, setting it in the intersection area of geometric control theory and vortex dynamics, the problem is quite novel.

However, control of Hamiltonian cylinder-point vortex models per se is not a new idea and neither is the control objective we study. Previous approaches have considered the cylinder *fixed in place* in the flow of a uniform stream and are typically set in a non-geometric-control setting. Important examples are the work of Kadtke and Novikov [9], who were probably the first to consider the problem of the capture of a point vortex, i.e. changing its orbit type from scattering to bound (the vice-versa objective was not considered), Péntek, Kadtke and Pedrizzetti [17], Protas [20] and Li and Aubry [10]. It is worthwhile to emphasize the differences between these previous works and our model, namely: (i) our control-free model is a fully coupled model (within an inviscid framework) in which the cylinder is free to move under the action of the pressure field on it surface and is not held in place or constrained in any way, (ii) we make explicit use of geometric mechanics ideas such as Hamiltonian structure, symmetries and momentum maps to construct our control model and (iii) we consider optimal control using Pontryagin's maximum principle. It should also be pointed out that optimal control of idealized interacting fluid-solid systems has been considered before by [5, 6, 8] but in all those models there is zero vorticity in the flow. Some results on the time-optimal control and local accessibility of the model in this paper,

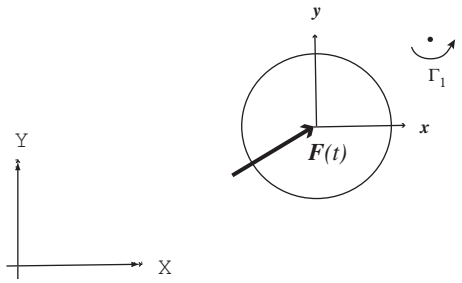

Figure 1: A 2D rigid circular cylinder dynamically interacting with one point vortex external to it and with a control force acting through its center of mass.

without invoking symmetries, may be found in [12].

The structure of the paper is as follows. In Section 2 we briefly review the SMBK Hamiltonian model for a circular cylinder and N vortices. In Section 3, for the case N=1 we implement the techniques of symplectic reduction and obtain the symmetry reduced spaces and Hamiltonian vector fields. In Section 4, we construct a single-input control system on the symplectic reduced space. The control input is a force acting through the cylinder center. In Section 5 we investigate both non-optimal and optimal control trajectories for this system with the control objective of changing the vortex orbit type from bound to scattering and vice versa. For the optimal control we use Pontryagin's maximum principle to minimize total impulse or 'fuel consumption' cost. Finally, in Section 6 a few concluding remarks are made and future directions discussed.

2 The SMBK model

In this section, some features of the SMBK model for general N which are relevant for the case $N = 1$ that is studied in this paper will be presented.

2.1 Equations of motion

Recall that in the SMBK model [26] the control-free equations of motion of a 2-D rigid circular cylinder dynamically interacting with N point vortices in an inviscid framework are:[1]

$$\frac{d\mathbf{L}}{dt} = -\mathbf{V} \times \Gamma \mathbf{k}, \tag{1}$$

$$\Gamma_j \frac{d\mathbf{l}_j}{dt} = -J \frac{\partial H}{\partial \mathbf{l}_j}, \quad j = 1, \ldots, N, \tag{2}$$

where $\mathbf{V}$ is the velocity of the body center of mass, $\mathbf{l}_j$ is the position vector of the jth point vortex in the body-fixed frame, $\mathbf{k}$ is the unit vector normal to the plane, $J = \begin{pmatrix} 0 & -1 \\ 1 & 0 \end{pmatrix}$ is the canonical symplectic matrix, Γ_j is the strength of the jth point vortex, $\Gamma = \sum_{j=1}^{N} \Gamma_j$ and $\mathbf{L}$ is the linear momentum of the system (i.e. fluid linear impulse plus cylinder linear momentum) given by:

$$\mathbf{L} = c\mathbf{V} + \sum_{j=1}^{N} \Gamma_j \mathbf{l}_j \times \mathbf{k} + R^2 \sum_{j=1}^{N} \mathbf{k} \times \Gamma_j \left(\frac{x_j}{x_j^2 + y_j^2}, \frac{y_j}{x_j^2 + y_j^2} \right). \tag{3}$$

In the above R is the radius of the cylinder and $c = 2\pi R^2$ denotes the mass plus the "added mass" of the cylinder. Note that due to the free-slip boundary conditions at the cylinder surface the angular velocity of the cylinder plays no role in the dynamics of the system.

The system state space is

$$P := (\mathbb{R}^2)^* \times (\mathbb{R}^{2N} \backslash (\triangle \cup B^N)) \equiv P_b \times P_v,$$

where $\triangle$ denotes the set of all collision configurations of the point vortices, i.e. configurations in which two or more vortices occupy the same point in the plane. B^N denotes

[1] All quantities in the equations are with reference to a body-fixed frame whose origin is at the body center-of-mass.

N copies of the region $B \cong S^1 \subset \mathbb{R}^2$ occupied by the body. The excluded set, $\triangle \cup B^N$, is therefore the set containing all collisions configurations of the vortices, amongst themselves and with the cylinder.

The Hamiltonian function H is the body+fluid kinetic energy minus infinity terms and is not explicitly written here for general N. For the case $N = 1$, it is written in the next section. The Poisson bracket structure is briefly discussed in Appendix A. For more details on all these see [26].

Notation for pairings

In the rest of this paper, the notation $\langle , \rangle$ stands for the canonical inner-product on Euclidean space $\mathbb{R}^N$, viewed, also, as the canonical pairing between $\mathbb{R}^N$ and its dual space $\left(\mathbb{R}^N\right)^*$.

3 Symmetry and reduction of the dynamics for $N = 1$

Consider the one point vortex case ($N = 1$). In this case, (1) and (2) represent a four dimensional system. Let $\mathbf{X} = (L_x, L_y, x_1, y_1)^T$, where the pairs L_x, L_y and x_1, y_1 are the components of $\mathbf{L}$ and $\mathbf{l_1}$, respectively.

The Hamiltonian function and the Poisson brackets now assume the following form:

$$H(\mathbf{L}, \mathbf{l}_1) = \frac{\Gamma_1^2}{4\pi} \log a + \frac{1}{c} \left(\frac{1}{2} \langle \mathbf{L}, \mathbf{L} \rangle - a \langle \mathbf{L} \times \Gamma_1 \mathbf{l}_1, \mathbf{k} \rangle + \frac{\Gamma_1^2}{2} a^2 \|\mathbf{l}_1\|^2 \right), \tag{4}$$

where $a(\|\mathbf{l}_1\|; R) = 1 - R^2/(\|\mathbf{l}_1\|^2)$, and

$$\{F, G\} := \Gamma_1 \left(\frac{\partial F}{\partial L_y} \frac{\partial G}{\partial L_x} - \frac{\partial F}{\partial L_x} \frac{\partial G}{\partial L_y} \right) + \frac{1}{\Gamma_1} \left(\frac{\partial F}{\partial x_1} \frac{\partial G}{\partial y_1} - \frac{\partial F}{\partial y_1} \frac{\partial G}{\partial x_1} \right),$$

respectively. Note that $0 < a < 1$. The Hamiltonian (4) is the kinetic energy of the body+fluid system *minus* infinite contributions. These contributions arise due to two standard reasons (see, for example, [2], §7.3): (i) the singular nature of the velocity field of the point vortices and (ii) the fact that the flow domain is unbounded.

The control-free vector field $\mathbf{f}(\mathbf{X}) = (f_1(\mathbf{X}), f_2(\mathbf{X}), f_3(\mathbf{X}), f_4(\mathbf{X}))^T$ is then given by:

$$f_1(\mathbf{X}) = -\Gamma_1 \frac{\partial H}{\partial L_y} = -\frac{\Gamma_1}{c}\left(L_y + \Gamma_1 x_1 a\right), \tag{5}$$

$$f_2(\mathbf{X}) = \Gamma_1 \frac{\partial H}{\partial L_x} = \frac{\Gamma_1}{c}\left(L_x - \Gamma_1 y_1 a\right), \tag{6}$$

$$\begin{aligned} f_3(\mathbf{X}) &= \frac{1}{\Gamma_1}\frac{\partial H}{\partial y_1}, \\ &= \frac{R^2}{\|\mathbf{l}_1\|^4}\left(\frac{L_x(x_1^2 - y_1^2) + 2L_y x_1 y_1}{c} + \frac{\Gamma_1}{2\pi}\frac{y_1}{a}\right) \\ &\qquad + \frac{1}{c}\left(-L_x + \Gamma_1 y_1 a(2-a)\right), \\ f_4(\mathbf{X}) &= -\frac{1}{\Gamma_1}\frac{\partial H}{\partial x_1}, \\ &= \frac{R^2}{\|\mathbf{l}_1\|^4}\left(\frac{L_y(y_1^2 - x_1^2) + 2L_x x_1 y_1}{c} - \frac{\Gamma_1}{2\pi}\frac{x_1}{a}\right) \\ &\qquad - \frac{1}{c}\left(L_y + \Gamma_1 x_1 a(2-a)\right). \end{aligned}$$

Note that since $\|\mathbf{l}_1\| > R > 0$, the vector field is C^∞ on P.

To formulate our control problem and to arrive at conclusions theoretically is, relatively speaking, difficult to do directly on the unreduced four-dimensional system. With this in mind, we try to exploit the Hamiltonian structure and symmetries in the system to reduce the system dimension and then formulate control problems directly on the symmetry reduces spaces.

Next, we give details of the symmetry reduction and obtain the symmetry reduced spaces. For an explanation of the ideas used in this section, including the differential geometric notation, the reader is referred to [11].

3.1 S^1-symmetry and momentum maps

The Hamiltonian function H and the Poisson bracket are invariant under the following diagonal action of the rotation group S^1 on P:

$$\Phi_A \cdot (\mathbf{L}, \mathbf{l}_1) = (A \cdot \mathbf{L}, A \cdot \mathbf{l}_1), \tag{7}$$

where $A \in \mathrm{SO}(2)$ and $\Phi_A : P \to P$ denotes the S^1 action of element $A \in \mathrm{SO}(2)$.

This diagonal S^1 action admits a momentum map, $\mathbf{J}_{S^1} : P \longrightarrow \mathfrak{g}^* \equiv \mathbb{R}^* \equiv \mathbb{R}$ computed in the standard fashion [11] i.e. the infinitesimal generator, $\xi_P(\mathbf{X})$, of the action should be a Hamiltonian vector field relative to the bracket and the Hamiltonian function defined by the $\mathbb{R}$-valued momentum map. The infinitesimal generator is easily computed as

$$\xi_P(\mathbf{X}) = (-L_y, L_x, -y_1, x_1)\xi$$

and the momentum map as

$$\mathbf{J}_{S^1}(\mathbf{X}) = \frac{1}{2}\left(\frac{\|\mathbf{L}\|^2}{\Gamma_1} - \Gamma_1 \|\mathbf{l}_1\|^2\right).$$

By Noether's Theorem, this quantity is conserved by the dynamics. Note that both the group action and the momentum map can be generalized in a straightforward manner for general N for the case $\Gamma := \sum_i^N \Gamma_i \neq 0$.

3.1.1 Symplectic Reduction

In terms of p and q (see Appendix C), the momentum map is

$$\mathbf{J}_{S^1}(\mathbf{X}) = \frac{1}{2}\left(\frac{\|\mathbf{L}\|^2}{\Gamma_1} - \Gamma_1 \|\mathbf{l}_1\|^2\right) = \frac{p}{\Gamma_1} - \Gamma_1 q = \mu \tag{8}$$

Choose (p,ϕ,θ) as coordinates for $\mathbf{J}_{S^1}^{-1}(\mu)$, where ϕ and θ are angle coordinates in the physical plane of the vectors $\mathbf{L}$ and $\mathbf{l}$, respectively.

The inclusion map $i_\mu : \mathbf{J}_{S^1}^{-1}(\mu) \longrightarrow P$ is given, using polar coordinates for P, by

$$i_\mu(p,\phi,\theta) = (p,(1/\Gamma_1)(p/\Gamma_1-\mu),\phi,\theta).$$

Since P is also a symplectic manifold with symplectic form given by

$$\Omega = \frac{1}{\Gamma_1} d\phi \wedge dp + \Gamma_1 dq \wedge d\theta,$$

the inclusion map defines a presymplectic form on $\mathbf{J}_{S^1}^{-1}(\mu)$ by pullback:

$$i_\mu^* \Omega = \frac{1}{\Gamma_1}(-dp \wedge d\phi + dp \wedge d\theta)$$

The symmetry group that acts on $\mathbf{J}_{S^1}^{-1}(\mu)$ is also S^1 since it is Abelian (i.e the coadjoint isotropy group is the full group). The projection map $\pi_\mu : \mathbf{J}_{S^1}^{-1}(\mu) \longrightarrow P_\mu$, where

$$P_\mu = \mathbf{J}_{S^1}^{-1}(\mu)/S^1,$$

is given in coordinates by $\pi_\mu(p,\phi,\theta) = (p,\alpha)$, where $\alpha = \phi - \theta$.

The symplectic form Ω_μ on P_μ defined by [13]

$$i_\mu^* \Omega = \pi_\mu^* \Omega_\mu,$$

is then given by

$$\Omega_\mu = \frac{1}{\Gamma_1}(-dp \wedge d\alpha)$$

Next, we obtain the reduced Hamiltonian $h_\mu : P_\mu \longrightarrow \mathbb{R}$ by restriction of (4):

$$h_\mu(p,\alpha) = \frac{\Gamma_1^2}{4\pi} \log\left(\frac{b}{2p_\mu}\right) \tag{9}$$

$$+ \frac{1}{c}\left(p + b\sqrt{\frac{p}{p_\mu}}\sin\alpha + \frac{1}{4}\frac{b^2}{p_\mu}\right), \tag{10}$$

where $b = 2p_\mu - \Gamma_1^2 R^2$ and $p_\mu = p - \Gamma_1 \mu$. Note the following inequalities,

$$p_\mu > \frac{\Gamma_1^2 R^2}{2} > 0, \quad b > 0, \quad 0 < \frac{b}{2p_\mu} < 1 \tag{11}$$

Reduced Hamiltonian Vector Field: The Hamiltonian vector field on P_μ is obtained as

$$\begin{aligned}
\frac{dp}{dt} &= -\Gamma_1 \frac{\partial h_\mu}{\partial \alpha}, \\
&= -\frac{\Gamma_1}{c} b \sqrt{\frac{p}{p_\mu}} \cos\alpha, \qquad (12) \\
\frac{d\alpha}{dt} &= \Gamma_1 \frac{\partial h_\mu}{\partial p}, \\
&= \frac{\Gamma_1^5 R^2}{4\pi b p_\mu} + \frac{\Gamma_1}{c}\left(\sqrt{\frac{p}{p_\mu}} + \sqrt{\frac{p_\mu}{p}} - \frac{\Gamma_1^2 R^2}{2p_\mu}\left(\sqrt{\frac{p_\mu}{p}} - \sqrt{\frac{p}{p_\mu}}\right)\right)\sin\alpha \\
&\qquad + \frac{\Gamma_1}{c}\left(2 - \frac{\Gamma_1^4 R^4}{4p_\mu^2}\right) \qquad (13)
\end{aligned}$$

The trajectories of (12) and (13) are given by the level curves of the reduced Hamiltonian function h_μ and are shown in Figure 2.

4 Control system on the symplectic symmetry reduced space

In the presence of a control input in the form of an external force **F** acting through the center of mass of the body(≡ centroid ≡ origin of body-fixed frame), as shown in Figure 1, the equations of motion (1) and (2) in the unreduced space become:

$$\frac{d\mathbf{L}}{dt} = -\mathbf{V} \times \Gamma \mathbf{k} + \mathbf{F}, \tag{14}$$

$$\Gamma_j \frac{d\mathbf{l}_1}{dt} = -J \frac{\partial H}{\partial \mathbf{l}_1}, . \tag{15}$$

The system (14) and (15) can be re-written in the form of a 4-dimensional affine control system [16]:

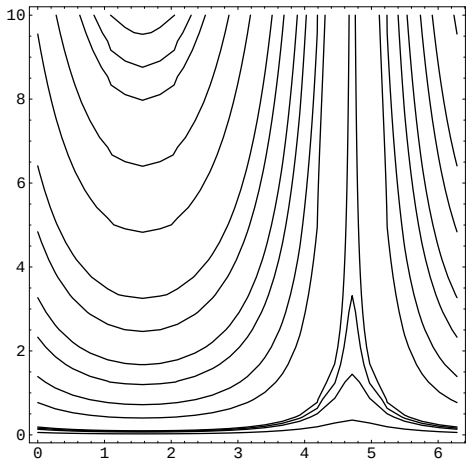

Figure 2: Level curves of the reduced Hamiltonian function h_μ for the following parameter values $R = 1, \Gamma_1 = 1$ and $\mu = -0.75$. The *y*-axis represents p and the *x*-axis represents α. The levels of the curves decrease in value going down the *y*-axis.

$$\frac{d\mathbf{X}}{dt} = \mathbf{f}(\mathbf{X}) + \mathbf{G}(\mathbf{X})\mathbf{u}, \tag{16}$$

where $\mathbf{G} = (\mathbf{g}_1, \mathbf{g}_2)$ and $\mathbf{g}_1$ and $\mathbf{g}_2$ are, in general, 4-dimensional vector fields. The vector $\mathbf{u} = (u_1, u_2)^T$ is the control input vector with elements u_1 and u_2 being the components of the external force $\mathbf{F}$ in the *x* and *y* directions respectively.

To formulate an S^1-invariant control system which leaves the momentum map invariant, we stipulate that the force vector field $X_F = (F_x, F_y, 0, 0) : P \to TP$ on P be S^1-invariant, i.e. it should satisfy

$$X_F(A \cdot \mathbf{X}) = \mathbf{D}\Phi_A \cdot X_F(\mathbf{X}) = A \cdot X_F(\mathbf{X})$$

where $\mathbf{D}\Phi_A : TP \to TP$ denotes the derivative of the S^1 action (7). The last equality follows since, for this S^1 action, the derivative map $\mathbf{D}\Phi_A \equiv \Phi_A$.

To proceed further down to the reduced space P_μ, the force vector field on P should

not only be S^1-invariant but should also leave the momentum map value invariant. For the momentum map (8) to be invariant under the control system vector field $X_{\mathscr{C}}$, the following must be satisfied

$$\mathscr{L}_{X_{\mathscr{C}}} \mathbf{J}_{S^1} = 0,$$

where $\mathscr{L}$ denotes the Lie derivative. However,

$$\mathscr{L}_{X_{\mathscr{C}}} \mathbf{J}_{S^1} = \mathscr{L}_{X_H} \mathbf{J}_{S^1} + \mathscr{L}_{X_F} \mathbf{J}_{S^1}$$

where X_H is the Hamiltonian vector field on the unreduced space P. Since X_H leaves the momentum map invariant, it follows that

$$\mathscr{L}_{X_{\mathscr{C}}} \mathbf{J}_{S^1} = \mathscr{L}_{X_F} \mathbf{J}_{S^1} = \frac{2}{\Gamma_1} \langle \mathbf{F}, \mathbf{L} \rangle .$$

And thus we arrive at the following constraint for the force field to leave the momentum map invariant under the flow of (14) and (15):

$$\langle \mathbf{F}, \mathbf{L} \rangle = 0$$

If we ignore the trivial option, then this implies that the force must always be perpendicular to the $\mathbf{L}$ vector.

To summarize, in order to obtain a control system directly on the reduced space P_μ, the following two conditions are sufficient: (i) the force field is S^1-invariant and (ii) the force vector $\mathbf{F}$ is always perpendicular to the linear momentum vector $\mathbf{L}$.

Note that in polar coordinates the force terms take the following form on the unreduced space: $\langle \mathbf{F}, \mathbf{L} \rangle / \|\mathbf{L}\|$ and $(\mathbf{L} \times \mathbf{F})/\|\mathbf{L}\|^2$, and appear on the right sides of equations (44) and (45), respectively. After imposing the above momentum map constraint on the force, the former term disappears and the latter term can be written as

$\pm\|\mathbf{F}\|/(2\sqrt{p})$, the sign depending on whether $\mathbf{F}$ is rotated 90° counter-clockwise or clockwise from $\mathbf{L}$.

Thus, we obtain the following S^1-invariant single-input affine control system (without any momentum map constraint) on the reduced space P_μ:

$$\frac{dp}{dt} = X^p_{h_\mu} \tag{17}$$

$$\frac{d\alpha}{dt} = X^\alpha_{h_\mu} + \frac{u}{2\sqrt{p}} \tag{18}$$

where $X^p_{h_\mu}$ and $X^\alpha_{h_\mu}$ are the components of the drift vector field (right sides of equations (12) and (13) respectively) and $u = \pm\|\mathbf{F}\|$. Writing it in the form of (16) and introducing the notation $\mathbf{X}_\mu \equiv (p,\alpha) \in P_\mu$, we see that $\mathbf{G}(\mathbf{X}_\mu) = \mathbf{g}(\mathbf{X}_\mu) = (0, 1/(2\sqrt{p}))$ consists of just a single vector for this system.

5 Vortex capture and vortex scattering on momentum level sets

It is obvious from Figure 2 that the vortex orbits relative to the moving cylinder are either bound orbits or scattering orbits. Examples of such orbits in the physical plane are shown in Figures 3 and 4. In this section, we discuss control laws to change the vortex orbit from one type to another. Before proceeding, we pause to introduce the following standard notation for concatenation of curves [27] to be used later.

Notation Given curves $d_1 : [t_0, t_1] \to \mathbb{R}^N$ and $d_2 : [t_1, t_2] \to \mathbb{R}^N$ where $t_0 \le t_1 \le t_2$, the curve

$$d = d_2 \star d_1,$$

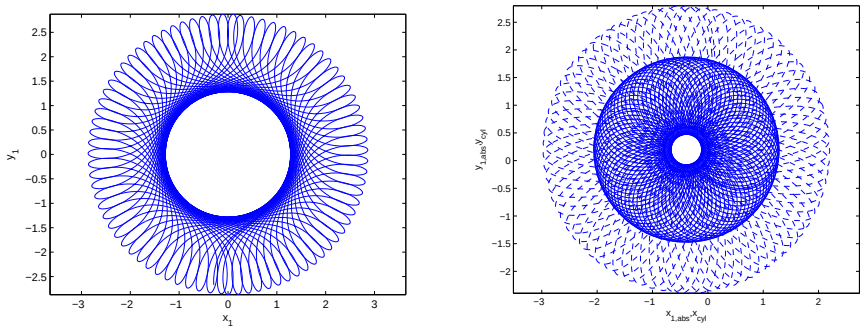

Figure 3: Bound vortex and cylinder orbits for parameter values: $R = 1, \Gamma_1 = 1$, $\mu = -0.75$ and $k = -0.01$. The plot on the left shows the orbit of the vortex in the body-fixed frame of the moving cylinder and the plot on the right shows the cylinder orbit (dashed) and vortex orbit in a spatially fixed frame.

is defined as

$$d(t) = d_1(t), \quad t \in [t_0, t_1),$$

$$= d_2(t), \quad t \in [t_1, t_2].$$

The control objectives for vortex capture and vortex scattering in the S^1-invariant control system X_C on P_μ, given by (17) and (18), are now stated.

Control objective for vortex capture: *To design a controller that will move the vortex from a given point in a scattering orbit of energy-momentum value* (k_1, μ) *to a point in a bound orbit of energy-momentum value* (k_2, μ).

Control objective for vortex scattering: *To design a controller that will move the vortex from a given point in a bound orbit of energy-momentum value* (k_1, μ) *to a point in a scattering orbit of energy-momentum value* (k_2, μ).

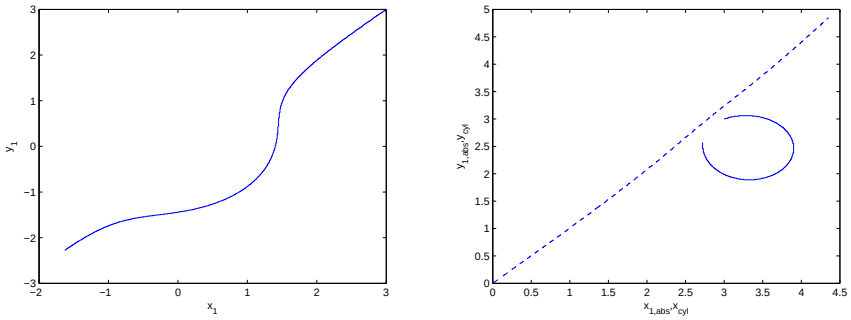

Figure 4: Scattering vortex and cylinder orbits for parameter values: $R = 1, \Gamma_1 = 1$, $\mu = -0.75$ and $k = 0.031$. The plot on the left shows the orbit of the vortex in the body-fixed frame of the moving cylinder and the plot on the right shows the cylinder orbit (dashed) and vortex orbit in a spatially fixed frame.

5.1 Control without optimality criteria ('brute force' control)

In this subsection, we first look at how to achieve the above stated control objectives with no bounds on the control force and no optimality criterion.

Scattering orbit to bound orbit with $dp/dt < 0$ at initial time: We first address the case of transferring the vortex from a scattering orbit to a bound orbit when the initial point on the control trajectory has $dp/dt < 0$. Without controls, the value of dp/dt reaches zero and continues to positive values as the vortex swings past the point of minimum approach. It is obvious from (12) and Figure 2, that for such a point α changes continuously from $(\pi/2)^-$ to $(\pi/2)^+$.

In general, a control input with the following sufficient (but not necessary) feature can steer the system to satisfy the stated control objective: the control trajectory moves down in the k-p plane while maintaining α between $-\pi/2$ and $\pi/2$. From (12) it follows that such a control trajectory will eventually hit the contour curve, in Figure 2, at the required energy level k_2 of the desired bound orbit of the vortex.

This feature can be achieved by, for example, a controller for which

$$\left(\frac{d\alpha}{dt}\right)_C = 0, \tag{19}$$

with a control input of the form

$$u = -2\sqrt{p}X^{\alpha}_{h_\mu}. \tag{20}$$

and the closed loop control system is described by the equations

$$\left(\frac{dp}{dt}\right)_C = -\frac{\Gamma_1}{c} b \sqrt{\frac{p}{p_\mu}} \cos\alpha_0,$$
$$\left(\frac{d\alpha}{dt}\right)_C = 0.$$

Scattering orbit to bound orbit with $dp/dt > 0$ at initial time: It is obvious from Figure 2 that in this case α, at initial time, lies in the interval $\pi/2 < \alpha < 3\pi/2$. Thus, one can initially have a control input whose objective is to change dp/dt from a positive value to a negative value which can be achieved by decreasing α from its initial value greater than $\pi/2$ to a value less than $\pi/2$. Once this has been achieved the control input (20) can be implemented.

Therefore, an example of a control input in this case is,

$$u = u_2 \star u_1,$$

where u_1 is any control input that satisfies, at each time instant that it is on, the *inequality*

$$u_1 < -2\sqrt{p}X^{\alpha}_{h_\mu},$$

and u_2 is of the same form as (20). If t_0 denotes initial time, t_1 denotes the time when u_2 is turned on and t_2 denotes the final time, then the closed loop control system is

described by the equations:

$$\left(\frac{dp}{dt}\right)_C = -\frac{\Gamma_1}{c} b\sqrt{\frac{p}{p_\mu}}\cos\alpha,\, t\in[t_0,t_1),\ :\ \left(\frac{dp}{dt}\right)_C = -\frac{\Gamma_1}{c} b\sqrt{\frac{p}{p_\mu}}\cos\alpha_1,\, t\in[t_1,t_2]$$
$$\left(\frac{d\alpha}{dt}\right)_C = u_1 + 2\sqrt{p}X^\alpha_{h_\mu},\, t\in[t_0,t_1),\ :\ \left(\frac{d\alpha}{dt}\right)_C = 0,\, t\in[t_1,t_2],$$

where $\alpha_1 = \alpha(t_1)$.

Bound orbit to scattering orbit with $dp/dt > 0$ at initial time: In this case, α at initial time lies between $\pi/2$ and $3\pi/2$ and it is obvious, referring to (12) and Figure 2, that the control input can again be of the form (20). Note that there is really no need to consider separately the case $dp/dt < 0$ at initial time due to the periodicity in the sign of dp/dt in the bound orbit. One can allow an initial uncontrolled stage to allow for the sign of dp/dt to change to positive.

5.2 Optimal control and some 'bang-bang' non-optimal cases

We now consider optimal control of the problems discussed in the previous subsection and also discuss some 'bang-bang' non-optimal cases.

The Pontryagin Hamiltonian [19, 18] for the control system (17) and (18) is given by:

$$H_P(\mathbf{X}_\mu,\lambda,u) = \lambda^T X_{h_\mu} + \lambda^T \mathbf{g}(\mathbf{X}_\mu)u + \lambda_0 f_0,$$

where $\lambda = (\lambda_1,\lambda_2)$ is the adjoint vector satisfying the equations

$$\begin{aligned}\frac{d\lambda_1}{dt} &= -\frac{\partial H_P}{\partial p}\\ &= -\frac{\partial X^p_{h_\mu}}{\partial p}\lambda_1 - \left(\frac{\partial X^\alpha_{h_\mu}}{\partial p} + u\frac{\partial}{\partial p}\left(\frac{1}{2\sqrt{p}}\right)\right)\lambda_2 - \frac{\partial f_0}{\partial p}\lambda_0, \qquad (21)\\ \frac{d\lambda_2}{dt} &= -\frac{\partial H_P}{\partial \alpha} = -\frac{\partial X^p_{h_\mu}}{\partial \alpha}\lambda_1 - \frac{\partial X^\alpha_{h_\mu}}{\partial \alpha}\lambda_2 - \frac{\partial f_0}{\partial \alpha}\lambda_0, \qquad (22)\end{aligned}$$

λ_0 is a non-positive constant and the cost function $J = \int_{t_1}^{t_2} f_0(\mathbf{X}_\mu, u)\, dt$.

Total impulse or 'fuel' cost. Consider now the point-to-point transfer problem from specified point $\mathbf{X}_1$, on energy-momentum level (k_1, μ), at specified initial time t_1 to unspecified point $\mathbf{X}_2$, on energy-momentum level (k_2, μ), at unspecified final time t_2 with bounded u ($-1 \leq u \leq 1$). Moreover, we choose $f_0(\mathbf{X}_\mu, u) = \mid u \mid$ so that the cost function being minimized is the total impulse

$$J = \int_{t_1}^{t_2} \mid u \mid \; dt$$

The Pontryagin Hamiltonian, taking $\lambda_0 = -1$ (the case of abnormal controllers, $\lambda_0 = 0$, is discussed briefly later), becomes

$$\begin{aligned} H_P(\mathbf{X}_\mu, \lambda, u) &= \lambda^T X_{h_\mu} + \lambda^T \mathbf{g}(\mathbf{X}_\mu) u - \mid u \mid, \\ &= \lambda_1 X_{h_\mu}^p + \lambda_2 X_{h_\mu}^\alpha + \frac{\lambda_2}{2\sqrt{p}} u - \mid u \mid \end{aligned} \tag{23}$$

A necessary condition for an extremal $(\mathbf{X}_\mu^*, \lambda^*, u^*)$ is that it maximize H_P with respect to u. This implies that

$$u^* = 1, \quad \text{when } \frac{\lambda_2^*}{2\sqrt{p^*}} > 1, \tag{24}$$

$$u^* = 0, \quad \text{when } -1 \leq \frac{\lambda_2^*}{2\sqrt{p^*}} \leq 1, \tag{25}$$

$$u^* = -1, \quad \text{when } \frac{\lambda_2^*}{2\sqrt{p^*}} < -1, \tag{26}$$

$$0 < u^* < 1, \quad \text{when } \frac{\lambda_2^*}{2\sqrt{p^*}} = 1, \tag{27}$$

$$-1 < u^* < 0, \quad \text{when } \frac{\lambda_2^*}{2\sqrt{p^*}} = -1, \tag{28}$$

Following the terminology in time-optimal control, we will refer to the controller in the last two cases as *singular* controllers.

Transversality conditions The actual point $\mathbf{X}_2$ on the target energy-momentum level set (curve) (k_2, μ) at which the controller is turned off is determined by the transversality conditions:

$$(\lambda^*(\mathbf{X}_2(t_2)))^T \mathbf{t}(\mathbf{X}_2(t_2)) = 0,$$

where $\mathbf{t}$ denotes the unit tangent vector field on the target energy-momentum level curve. But since this curve is a level curve of h_μ, indeed an integral curve of the control-free vector field, it follows that $\mathbf{t}$ is parallel to X_{h_μ} at all points on the curve so the transversality condition becomes equivalent to

$$(\lambda^*(\mathbf{X}_2(t_2)))^T X_{h_\mu}(\mathbf{X}_2(t_2)) = 0$$

From (23) and the zero value of H_P along extremal trajectories it follows that at the final point

$$\frac{|\lambda_2^*|}{2\sqrt{p^*}} = 1, \tag{29}$$

if $u^* = \pm 1$ at the moment the controller is turned off. Note that the transversality condition is automatically satisfied by a singular extremal.

In Figure 5, the trajectories of the control system in the (p, α)-plane for the boundary values of u are shown. These curves are obtained as level curves of the control Hamiltonian functions defined as

$$h_\mu^+(p,\alpha) = \frac{\Gamma_1^2}{4\pi}\log\left(\frac{b}{2p_\mu}\right) + \frac{1}{c}\left(p + b\sqrt{\frac{p}{p_\mu}}\sin\alpha + \frac{1}{4}\frac{b^2}{p_\mu}\right) + \frac{\sqrt{p}}{\Gamma_1},$$
$$h_\mu^-(p,\alpha) = \frac{\Gamma_1^2}{4\pi}\log\left(\frac{b}{2p_\mu}\right) + \frac{1}{c}\left(p + b\sqrt{\frac{p}{p_\mu}}\sin\alpha + \frac{1}{4}\frac{b^2}{p_\mu}\right) - \frac{\sqrt{p}}{\Gamma_1}$$

Before studying optimal trajectories, we look briefly at 'bang-bang' *non-optimal* control ($u = \pm 1$) .

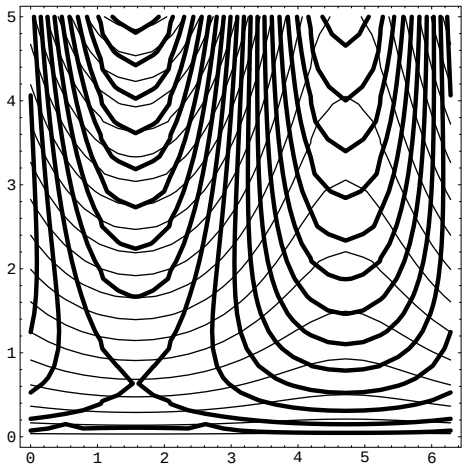

Figure 5: Level curves of the functions h_μ^+ (thin line) and h_μ^- (thick line) for the following parameter values: $R = 1, \Gamma_1 = 1$ and $\mu = -0.75$. The *y*-axis represents p and the *x*-axis represents α.

'Bang-bang' non-optimal control: scattering orbit to bound orbit From Figure 2, it is obvious that for the vortex to be placed on a bound orbit of some specified energy level it is sufficient for the control trajectory to hit the vertical line $\alpha = 3\pi/2$ (in the p-α plane) at the peak value p_{max} of the bound orbit. From Figure 5 it is easily seen that this can be achieved by a 'bang-bang' controller with at most one switch i.e by a control trajectory of the form

$$\gamma = \gamma_{-1} \star \gamma_{+1},$$

where γ_{+1} is the control trajectory, with $u = +1$, starting from the initial point (p_0, α_0) on the scattering orbit and γ_{-1} is the control trajectory, with $u = -1$, passing through the final point $(p_{max}, 3\pi/2)$, provided these two trajectories intersect. [2] As seen from Figures 2 and 5, these intersections do indeed occur for a large number of trajectories. However, if p_{max} lies below the separatrix of the γ_{-1} trajectories then such a bound

[2]Keeping in mind the directions of the control trajectories in Figure 5, it should also be noted that the switch occurs at a point right of the vertical line $\alpha = 3\pi/2$.

orbit may be inaccessible from a scattering orbit using 'bang-bang' control.

'Bang-bang' non-optimal control: bound orbit to scattering orbit Similar considerations apply but with the order of the control trajectories switched. Assuming the 'peak' of the bound orbit (see Figure 2) is above the separatrix of the γ_{-1} trajectories a control trajectory of the form

$$\gamma = \gamma_{+1} \star \gamma_{-1},$$

where γ_{-1} is the control trajectory starting from the initial point (p_0, α_0) on the bound orbit and γ_{+1} is the control trajectory passing through the final point (p_1, α_1), achieves the desired transfer.

5.2.1 Optimal and almost optimal control

From (24), (26), (25), (27) and (28), it follows that an extremal trajectory should be a concatenation of 'bang-bang', singular and control-free arcs.[3]

'Bang-bang' extremal arcs. A feature of extremal trajectories is that H_P is zero along extremals. Thus, for the boundary values of u^*,

$$H_P(\mathbf{X}^*_\mu, \lambda^*, u^* = \pm 1) = \lambda_1^* X_{h_\mu}^{p^*} + \lambda_2^* X_{h_\mu}^{\alpha^*} + \frac{|\lambda_2^*|}{2\sqrt{p^*}} - 1 = 0, \tag{30}$$

implies that

$$\begin{aligned} \lambda_1^* &= \frac{1}{X_{h_\mu}^{p^*}} \left(1 - \left(\lambda_2^* X_{h_\mu}^{\alpha^*} + \frac{|\lambda_2^*|}{2\sqrt{p^*}}\right)\right), \\ &= F(\lambda_2^*, X_{h_\mu}^{p^*}(p^*, \alpha^*), X_{h_\mu}^{\alpha^*}(p^*, \alpha^*), p^*), \end{aligned} \tag{31}$$

[3] Note that in this subsection, we will also be referring to the corresponding arcs of optimal trajectories in the p-α plane.

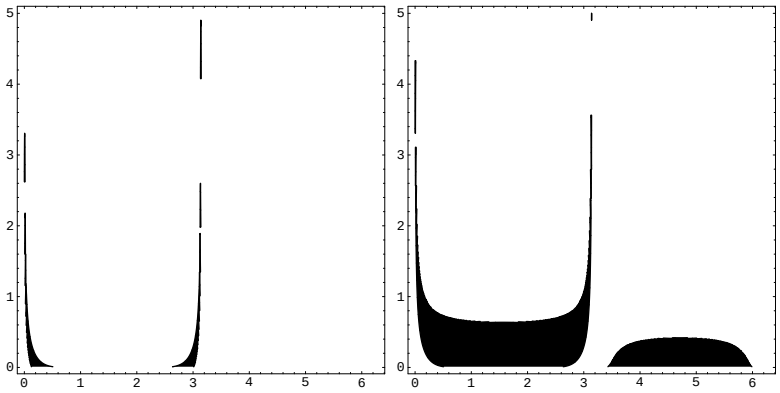

Figure 6: Black regions defining the domains in which the optimal control trajectory can lie for the normal 'bang-bang' case, with $u^* = 1$ in the left plot and $u^* = -1$ in the right plot, for the following parameter values: $R = 1, \Gamma_1 = 1$ and $\mu = -0.75$. The y-axis represents p and the x-axis represents α.

assuming $X_{h_\mu}^{p^*} \neq 0$.[4] Simultaneous satisfaction of (31) and the adjoint equations (21) and (22) written for the extremal, gives relations between the adjoint vectors and the state vectors along an extremal trajectory when $u^* = \pm 1$. In other words, along a 'bang-bang' extremal arc,

$$\lambda_1^* = \lambda_1^*\left(p^*, \alpha^*, u^* = \pm 1\right),$$

$$\lambda_2^* = \lambda_2^*\left(p^*, \alpha^*, u^* = \pm 1\right).$$

Only the second pair of these relations is important since the sign of λ_2^* determines the value of the optimal controller u^*. These relations are given in Appendix B1.

A 'bang-bang' extremal arc necessarily has to satisfy (24), (26), (42) and (43). The black regions, D_+ and D_- in the left and right plots in Figure 6, respectively, are the regions in the p-α plane where $(\lambda_2^*)^+/(2\sqrt{p^*}) > 1$ with $u^* = 1$ and $(\lambda_2^*)^-/(2\sqrt{p^*}) < -1$ with $u^* = -1$. It follows that a γ_{+1} arc of an optimal trajectory can occupy only

[4]This is an assumption we will make throughout this section since the case $X_{h_\mu}^{p^*} = 0$ does not give rise to any non-trivial optimal arcs.

D_+, a γ_{-1} arc of an optimal trajectory can occupy only D_- and both γ_{+1} and γ_{-1} arcs can occupy $D_+ \cap D_-$ if non-empty.

The imposition of the transversality condition (29) is equivalent to fixing the final point of the optimal trajectory as the point of intersection of the target curve with the boundaries of D_+ (if $u^* = 1$ at the moment the controller is turned off) or with the boundaries of D_- (if $u^* = -1$ at the moment the controller is turned off). However, not all boundaries of the black regions in Figure 6 are regular boundaries i.e boundaries across which $(\lambda_2^*)^+/(2\sqrt{p^*})$ and $(\lambda_2^*)^-/(2\sqrt{p^*})$ change *continuously*. The values of $(\lambda_2^*)^-/(2\sqrt{p^*})$ and $(\lambda_2^*)^+/(2\sqrt{p^*})$ blow up to positive and negative infinity as one approaches from either side, respectively, the inner boundaries in the left plot and the top boundaries of the black 'cup' and 'dome' in the right plot of Figure 6. Hence, a 'bang-bang' arc has to end on the outer boundaries of the left plot, where $(\lambda_2^*)^+/(2\sqrt{p^*}) = 1$, or on the bottom boundary of the black 'cup' in the right plot, where $(\lambda_2^*)^-/(2\sqrt{p^*}) = -1$, to satisfy the transversality condition.

Singular extremal arcs. For the singular controller cases,

$$\lambda_2^* = \pm 2\sqrt{p^*}, \quad \lambda_1^* = \mp 2\sqrt{p^*} X_{h_\mu}^{\alpha^*} / X_{h_\mu}^{p^*} \tag{32}$$

Substituting each $(\lambda_1^*, \lambda_2^*)$ pair in (21) gives, in both cases, a relation of the form

$$u^*\left(\frac{1}{2p^*}+\left(\frac{1}{X_{h_\mu}^{p^*}}\frac{\partial X_{h_\mu}^{\alpha^*}}{\partial\alpha^*}-\frac{X_{h_\mu}^{\alpha^*}}{\left(X_{h_\mu}^{p^*}\right)^2}\frac{\partial X_{h_\mu}^{p^*}}{\partial\alpha^*}\right)\right)$$
$$=-2\sqrt{p^*}X_{h_\mu}^{\alpha^*}\left(\frac{1}{2p^*}+\left(\frac{1}{X_{h_\mu}^{p^*}}\frac{\partial X_{h_\mu}^{\alpha^*}}{\partial\alpha^*}-\frac{X_{h_\mu}^{\alpha^*}}{\left(X_{h_\mu}^{p^*}\right)^2}\frac{\partial X_{h_\mu}^{p^*}}{\partial\alpha^*}\right)\right), \tag{33}$$

$$\Rightarrow u^*=-2\sqrt{p^*}X_{h_\mu}^{\alpha^*}, \quad \text{if } \frac{1}{2p^*}+\left(\frac{1}{X_{h_\mu}^{p^*}}\frac{\partial X_{h_\mu}^{\alpha^*}}{\partial\alpha^*}-\frac{X_{h_\mu}^{\alpha^*}}{\left(X_{h_\mu}^{p^*}\right)^2}\frac{\partial X_{h_\mu}^{p^*}}{\partial\alpha^*}\right)\neq 0,$$

valid when $0\leq \mid u^* \mid \leq 1$, and

$$u^*=\text{indeterminate}, \quad \text{if } \frac{1}{2p^*}+\left(\frac{1}{X_{h_\mu}^{p^*}}\frac{\partial X_{h_\mu}^{\alpha^*}}{\partial\alpha^*}-\frac{X_{h_\mu}^{\alpha^*}}{\left(X_{h_\mu}^{p^*}\right)^2}\frac{\partial X_{h_\mu}^{p^*}}{\partial\alpha^*}\right)=0. \tag{34}$$

Substituting (32) in (22) on the other hand gives a relation (curve in the p-α plane) $C(p^*,\alpha^*)=0$ of the form

$$C(p^*,\alpha^*):=\frac{2\sqrt{p^*}X_{h_\mu}^{\alpha^*}}{X_{h_\mu}^{p^*}}\frac{\partial X_{h_\mu}^{p^*}}{\partial\alpha^*}-\frac{X_{h_\mu}^{p^*}}{\sqrt{p^*}}-2\sqrt{p^*}\frac{\partial X_{h_\mu}^{\alpha^*}}{\partial\alpha^*}$$
$$=2\sqrt{p^*}X_{h_\mu}^{p^*}\left(\frac{X_{h_\mu}^{\alpha^*}}{\left(X_{h_\mu}^{p^*}\right)^2}\frac{\partial X_{h_\mu}^{p^*}}{\partial\alpha^*}-\frac{1}{2p^*}-\frac{1}{X_{h_\mu}^{p^*}}\frac{\partial X_{h_\mu}^{\alpha^*}}{\partial\alpha^*}\right)$$
$$=0. \tag{35}$$

It follows from (34) and (35) that the singular controller is indeterminate and a singular arc of the optimal trajectory has to coincide with (a portion of) the curve defined by (35) which is plotted in Figure 7. In Figure 8, the curves of Figure 2 and Figure 7 are shown superimposed.

Control-free extremal arcs. From Appendix B2, it follows that when λ_2^* is in the interval defined by (25) the arc of an optimal trajectory has to be a control-free arc or,

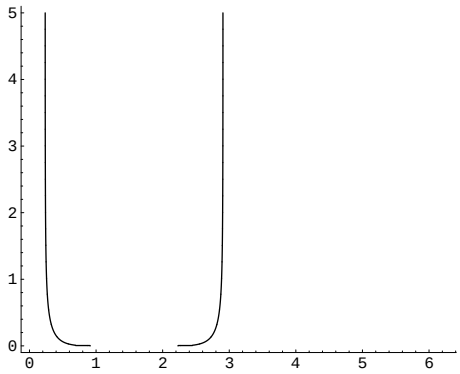

Figure 7: Singular optimal arcs for the following parameter values: $R = 1, \Gamma_1 = 1$ and $\mu = -0.75$. The *y*-axis represents p and the *x*-axis represents α.

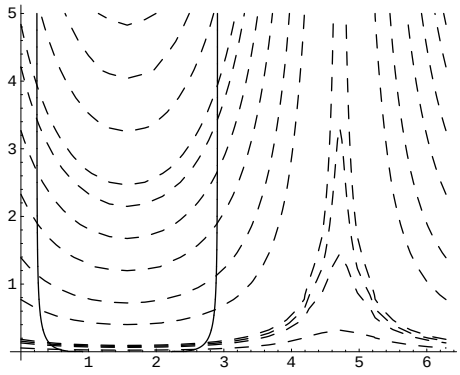

Figure 8: The singular optimal arcs of Figure 7 shown superimposed on the control-free trajectories of Figure 2 (shown dashed).

in other words, the arc of a level curve of the system shown in Figure 2. Obviously, for the control objectives of this paper, such an arc can lie only in the interior of the set of points of the optimal trajectory.

Abnormal controllers. For abnormal controllers, for which λ_0=0, the Pontryagin Hamiltonian (23) is

$$H_P(\mathbf{X}_\mu, \lambda, u) = \lambda_1 X^p_{h_\mu} + \lambda_2 X^\alpha_{h_\mu} + \frac{\lambda_2}{2\sqrt{p}} u. \tag{36}$$

It follows that optimal controllers in this case should be 'bang-bang'. Specifically, [5]

$$u^* = 1, \quad \text{when } \frac{\lambda_2^*}{2\sqrt{p^*}} > 0, \tag{37}$$

$$u^* = -1, \quad \text{when } \frac{\lambda_2^*}{2\sqrt{p^*}} < 0. \tag{38}$$

Analysis as in Appendix B gives the following two relations for λ_2^*

$$(\lambda_2^*)^+ \left(\frac{\partial X_{h_\mu}^{p^*}}{\partial \alpha^*} \left(X_{h_\mu}^{\alpha^*} + \frac{1}{2\sqrt{p^*}} \right) - X_{h_\mu}^{p^*} \frac{\partial X_{h_\mu}^{\alpha^*}}{\partial \alpha^*} \right) = 0, \quad u^* = 1,$$

$$(\lambda_2^*)^- \left(\frac{\partial X_{h_\mu}^{p^*}}{\partial \alpha^*} \left(X_{h_\mu}^{\alpha^*} - \frac{1}{2\sqrt{p^*}} \right) - X_{h_\mu}^{p^*} \frac{\partial X_{h_\mu}^{\alpha^*}}{\partial \alpha^*} \right) = 0, \quad u^* = -1$$

Since a zero value for λ_2^* is not allowed, it follows that abnormal 'bang-bang' extremal arcs should satisfy the relations

$$\left(\frac{\partial X_{h_\mu}^{p^*}}{\partial \alpha^*} \left(X_{h_\mu}^{\alpha^*} + \frac{1}{2\sqrt{p^*}} \right) - X_{h_\mu}^{p^*} \frac{\partial X_{h_\mu}^{\alpha^*}}{\partial \alpha^*} \right) = 0, \quad u^* = 1,$$

$$\left(\frac{\partial X_{h_\mu}^{p^*}}{\partial \alpha^*} \left(X_{h_\mu}^{\alpha^*} - \frac{1}{2\sqrt{p^*}} \right) - X_{h_\mu}^{p^*} \frac{\partial X_{h_\mu}^{\alpha^*}}{\partial \alpha^*} \right) = 0, \quad u^* = -1$$

The curves in the p-α plane defined by the above relations are in fact the boundaries of discontinuity (as discussed previously) of the black regions in Figure 6. These curves for the most part are not coincident with the control trajectories of the system for the boundary values of u^* shown in Figure 5.

Implementation issues. Before closing this section we briefly discuss some of the implementation issues involved with this model *within* this idealized framework i.e. without consideration of 3D, viscous and turbulence effects. The main issue obviously is the measurement of the state space variables $(\mathbf{L}, \mathbf{l}_1)$ and the parameter Γ_1. Since $\mathbf{L}$ is

[5] Note that the singular case here, i.e. $\lambda_2^* = 0$, implies $\lambda_1^* = 0$ from the zero value condition on (36) (see also footnote 4) and so is ruled out by the maximum principle.

related to $\mathbf{V}$ and $\mathbf{l}_1$ through (3), this is equivalent to the measurement of $(\mathbf{V}, \mathbf{l}_1)$ and Γ_1. Whereas the measurement of the cylinder velocity $\mathbf{V}$ is not an issue, the measurements of the vortex position (relative to the moving cylinder) $\mathbf{l}_1$ and the vortex strength Γ_1 require some discussion.

In flows represented by our model, it is obviously impractical to directly measure vortex characteristics from the moving body itself. In fact, even in more stationary situations such as laboratory flows, accurate tracking of a vortex requires a fairly elaborate diagnostic set-up involving illumination by laser sheets, seeding the flow, high-speed cameras etc. A more practical but indirect way of obtaining vortex information is to compute the pressure distribution around the body using pressure sensors located at different points on the body surface. Subtracting from this (total) pressure distribution the pressure distribution due to the irrotational flow associated with the motion of the body, [6] one obtains the pressure distribution due to the vortex flow. This pressure distribution can be used to estimate the location and strength of the vortex.

The change in direction of the control force can be achieved, in practice, by manipulation of aerodynamic surfaces on the body or by thrust vectoring.

Finally, we should mention that the control methodology and analysis presented in this paper can also be applied on the Poisson symmetry reduced space P/S^1 i.e. the symmetry reduced space without the constraint of the momentum map. However, the details of this case are not worked out in this paper.

[6] this pressure distribution can be obtained analytically for simple body geometries and numerically for others and depends only on the body shape and its instantaneous velocity, see [14]

6 Conclusions and future directions

Control of an idealized model of a fully coupled dynamically interacting planar fluid-solid system, in the presence of vorticity, is considered in this paper. In this model a circular cylinder interacts with a point vortex external to it. The control input is an external force acting through the center of the cylinder. Exploiting the Hamiltonian structure and symmetry in the problem, we are able to reduce the dimension of the system and formulate a control system directly on the symmetry reduced space. With the control objective of changing the vortex orbit type from bound to scattering and vice versa, both non-optimal and optimal control strategies are studied, the latter using Pontryagin's maximum principle.

A detailed investigation of the structure of the optimal control trajectories of the model revealed the following. Normal optimal control trajectories, in general, are combinations of 'bang-bang', singular and control-free arcs. The singular arcs, despite their simple structure, can achieve the desired control objective by themselves as shown in Figure 8. Moreover, the singular arcs connect orbits of many different energy levels. However, the singular controller is indeterminate. On the other hand, noting the almost vertical form of the singular arcs in Figure 8 and the analysis of 'brute-force' control in §5.1, it may be conjectured that a singular controller could be approximated by (20) in regions where $0 <\mid 2\sqrt{p}X^{\alpha}_{h_\mu} \mid< 1$. The 'bang-bang' arcs shown in Figure 5 have a restricted domain of validity in the p-α plane shown by the black regions in Figure 6. The $u^* = 1$ arcs lie in a very small domain making them for most purposes useless by themselves to achieve the control objective. The $u^* = -1$ arcs have a bigger domain of validity. In general, however, it can be seen that the 'bang-bang' controllers

are limited in their ability to achieve the desired vortex orbit transfer. Abnormal controllers are again 'bang-bang' but the corresponding control arcs are either trivial or have restricted use.

For future investigations in this idealized framework (but with applications in mind) the following extensions of this problem suggest themselves.

Non-circular cylinder shapes. For non-circular cylinder shapes the S^1-symmetry is broken. Moreover, the control free dynamics is also expected to be non-integrable. The control problem, with the same control objective, obviously becomes much more challenging in this case.

Control by shape changes. Equally challenging would be to have the shape of the cylinder as a control input rather than an external force. This would make the model more relevant to problems in biological and biomimetic locomotion (fish swimming, small autonomous underwater vehicles etc.). A swimming model of articulated rigid links in potential flow (no vorticity) was proposed by Radford [21] and studied further in [8].

Circular shapes, more vortices. Adding more vortices to the circular cylinder case and steering the cylinder in a 'sea' of vortices is another interesting problem. However, unless the vortices can be directly actuated the control system will be largely underactuated and the target set of a point in state space may be largely reduced. But for simple control objectives with no bounds on the control force or optimality criteria one can actually obtain results for any N number of vortices.

Appendix

A Poisson bracket structure

The system (1) and (2), in the variables $\mathbf{L}$ and $\mathbf{l}_j$ $(j = 1, ..., N)$, is Hamiltonian with respect to the following Poisson bracket on the state space P

$$\{F,G\} := \{F\mid_{P_v}, G\mid_{P_v}\}_{\text{point vortex}}, \quad \text{if}\,\Gamma = 0,$$

$$\{F,G\} = \{F\mid_{P_v}, G\mid_{P_v}\}_{\text{point vortex}} + \{F\mid_{P_b}, G\mid_{P_b}\}_{2-\text{cocycle}}, \quad \text{if}\,\Gamma \neq 0.$$

The component Poisson brackets in the above equations are as follows. The first bracket is the canonical point vortex bracket on the space $P_v \equiv (\mathbb{R}^{2N} \backslash (\triangle \cup B^N))$:

$$\{F\mid_{P_v}, G\mid_{P_v}\}_{\text{point vortex}} = \sum_{j=1}^{N} \left\langle \nabla_j F, J^{-1} \nabla_j (G/\Gamma_j) \right\rangle,$$

where ∇_j denotes the gradient operator with respect to $\mathbf{l}_j$.

The second component bracket, which arises only in the case $\Gamma \neq 0$, is on $(\mathbb{R}^2)^*$ and is given by:

$$\{F\mid_{P_b}, G\mid_{P_b}\}_{2-\text{cocycle}} = \Gamma \left(\frac{\partial F}{\partial L_y}\frac{\partial G}{\partial L_x} - \frac{\partial G}{\partial L_y}\frac{\partial F}{\partial L_x} \right) \tag{39}$$

This Poisson bracket is related to the 2-cocycle, which is a real-valued map on two copies of a Lie algebra and is defined when the momentum map of the related symmetry (Lie) group lacks the property of $\text{Ad}^* -$equivariance [11] (the property of commutability of the map with the given action of the symmetry group). The general theory behind this idea is stated in Abraham and Marsden [1]. A discussion on how this 2-cocycle bracket arises in this problem can be found in [25].

The equations (1) and (2) are then obtained in the usual manner. In other words,

for $p(t) = (\mathbf{L}(t), \mathbf{l}_j(t)) \in P$, an integral curve of the system,

$$\frac{dF}{dt} := \left\langle \nabla_p F, \frac{dp}{dt} \right\rangle = \{F, H\}$$

B $\lambda_2^*(p^*, \alpha^*)$

B.1 Normal 'bang-bang' extremals

$$\frac{d\lambda_1^*}{dt} = -\frac{\partial X_{h_\mu}^{p^*}}{\partial p^*}\lambda_1^* - \left(\lambda_2^* \frac{\partial X_{h_\mu}^{\alpha^*}}{\partial p^*} + \mid \lambda_2^* \mid \frac{\partial}{\partial p^*}\left(\frac{1}{2\sqrt{p^*}}\right)\right), \tag{40}$$

$$\frac{d\lambda_2^*}{dt} = -\frac{\partial X_{h_\mu}^{p^*}}{\partial \alpha^*}\lambda_1^* - \frac{\partial X_{h_\mu}^{\alpha^*}}{\partial \alpha^*}\lambda_2^*, \tag{41}$$

where $\frac{\partial X_{h_\mu}^{p^*}}{\partial p^*}$ stands for $\frac{\partial X_{h_\mu}^{p}}{\partial p}$ along the extremal trajectory and so on. Imposing the constraint (31), these equations become

$$\begin{aligned}
\frac{\partial F}{\partial \lambda_2^*}\frac{d\lambda_2^*}{dt} &+ \left(\frac{\partial F}{\partial X_{h_\mu}^{p^*}}\frac{\partial X_{h_\mu}^{p^*}}{\partial p^*} + \frac{\partial F}{\partial X_{h_\mu}^{\alpha^*}}\frac{\partial X_{h_\mu}^{\alpha^*}}{\partial p^*} + \frac{\partial F}{\partial p^*}\right) X_{h_\mu}^{p^*} \\
&+ \left(\frac{\partial F}{\partial X_{h_\mu}^{p^*}}\frac{\partial X_{h_\mu}^{p^*}}{\partial \alpha^*} + \frac{\partial F}{\partial X_{h_\mu}^{\alpha^*}}\frac{\partial X_{h_\mu}^{\alpha^*}}{\partial \alpha^*}\right) X_{h_\mu}^{\alpha^*} \\
&= -\frac{\partial X_{h_\mu}^{p^*}}{\partial p^*}F - \left(\lambda_2^* \frac{\partial X_{h_\mu}^{\alpha^*}}{\partial p^*} + \mid \lambda_2^* \mid \frac{\partial}{\partial p^*}\left(\frac{1}{2\sqrt{p^*}}\right)\right), \\
\frac{d\lambda_2^*}{dt} &= -\frac{\partial X_{h_\mu}^{p^*}}{\partial \alpha^*}F - \frac{\partial X_{h_\mu}^{\alpha^*}}{\partial \alpha^*}\lambda_2^*,
\end{aligned}$$

This gives a linear equation for λ_2^*

$$\begin{aligned}
&\frac{\partial X_{h_\mu}^{p^*}}{\partial \alpha^*}F + \frac{\partial X_{h_\mu}^{\alpha^*}}{\partial \alpha^*}\lambda_2^* \\
&= \frac{1}{\frac{\partial F}{\partial \lambda_2^*}}\left(\frac{\partial X_{h_\mu}^{p^*}}{\partial p^*}F + \left(\lambda_2^* \frac{\partial X_{h_\mu}^{\alpha^*}}{\partial p^*} + \mid \lambda_2^* \mid \frac{\partial}{\partial p^*}\left(\frac{1}{2\sqrt{p^*}}\right)\right)\right. \\
&\left. + \left(\frac{\partial F}{\partial X_{h_\mu}^{p^*}}\frac{\partial X_{h_\mu}^{p^*}}{\partial p^*} + \frac{\partial F}{\partial X_{h_\mu}^{\alpha^*}}\frac{\partial X_{h_\mu}^{\alpha^*}}{\partial p^*} + \frac{\partial F}{\partial p^*}\right) X_{h_\mu}^{p^*} + \left(\frac{\partial F}{\partial X_{h_\mu}^{p^*}}\frac{\partial X_{h_\mu}^{p^*}}{\partial \alpha^*} + \frac{\partial F}{\partial X_{h_\mu}^{\alpha^*}}\frac{\partial X_{h_\mu}^{\alpha^*}}{\partial \alpha^*}\right) X_{h_\mu}^{\alpha^*}\right),
\end{aligned}$$

Substituting for F and its derivatives, one obtains two equations for λ_2^*, one for $u^* = 1$,

$$\begin{aligned}(\lambda_2^*)^+ &:= \lambda_2^* \mid_{u^*=1} \\ &= \frac{\frac{\partial X_{h_\mu}^{p^*}}{\partial \alpha^*}}{\frac{\partial X_{h_\mu}^{p^*}}{\partial \alpha^*}\left(X_{h_\mu}^{\alpha^*} + \frac{1}{2\sqrt{p^*}}\right) - X_{h_\mu}^{p^*}\frac{\partial X_{h_\mu}^{\alpha^*}}{\partial \alpha^*}},\end{aligned} \tag{42}$$

and the other for $u^* = -1$

$$\begin{aligned}(\lambda_2^*)^- &:= \lambda_2^* \mid_{u^*=-1} \\ &= \frac{\frac{\partial X_{h_\mu}^{p^*}}{\partial \alpha^*}}{\frac{\partial X_{h_\mu}^{p^*}}{\partial \alpha^*}\left(X_{h_\mu}^{\alpha^*} - \frac{1}{2\sqrt{p^*}}\right) - X_{h_\mu}^{p^*}\frac{\partial X_{h_\mu}^{\alpha^*}}{\partial \alpha^*}},\end{aligned} \tag{43}$$

B.2 Normal control-free extremals

In this case, with $u^* = 0$, the relation (31) assumes the form

$$\lambda_1^* = -\frac{X_{h_\mu}^{\alpha^*}}{X_{h_\mu}^{p^*}}\lambda_2^*$$

which satisfies (40) and (41) identically and so, unlike in the 'bang-bang' case, one cannot identify domains in the p-α in which the control-free arcs of the optimal trajectory should lie.

C Polar Coordinates (p, ϕ, q, θ)

Introducing polar coordinates $\mathbf{r} = (p, \phi, q, \theta)$, where $p = \|\mathbf{L}\|^2/2$, $q = \|\mathbf{l_1}\|^2/2$, and writing $a = (1 - R^2/(2q))$, the unreduced vector field transforms as:

$$f_1(\mathbf{r}) = \frac{dp}{dt} = -\frac{2\Gamma_1^2}{c} a\sqrt{pq}\cos(\theta - \phi) \tag{44}$$

$$f_2(\mathbf{r}) = \frac{d\phi}{dt} = \frac{\Gamma_1^2}{c}\left(\frac{1}{\Gamma_1} - a\sqrt{\frac{q}{p}}\sin(\theta - \phi)\right) \tag{45}$$

$$f_3(\mathbf{r}) = \frac{dq}{dt} = -\frac{2}{c} a\sqrt{pq}\cos(\theta - \phi),$$

$$f_4(\mathbf{r}) = \frac{d\theta}{dt} = \left(\sqrt{\frac{p}{q}}(2-a)\sin(\theta - \phi) - \frac{\Gamma_1 R^2}{8\pi q^2 a} - \frac{\Gamma_1}{c} a(2-a)\right)$$

Since polar transformations are not defined at the origin the above equations indicate an apparent singularity in the vector field at $\|\mathbf{L}\| = 0$. This is not a genuine singularity of the vector field. System trajectories pass smoothly, in fact C^∞-smoothly, through points where $\mathbf{L} = 0$. To understand the system behavior at $\mathbf{L} = 0$ one has to go back to the equations written in the Cartesian coordinates.

References

[1] Abraham RH, Marsden JE [1987]. *Foundations of Mechanics*, Second Edition, Addison-Wesley, c1978, Sixth Printing, 1987, available online at http://resolver.caltech.edu/CaltechBOOK:1987.001

[2] Batchelor GK [1970], *An Introduction to Fluid Dynamics*. Cambridge University Press.

[3] Borisov AV, Mamaev IS and Ramodanov SM [2003]. Motion of a circular cylinder and *n* point vortices in a perfect fluid, *Reg. Chaotic Dyn.*, **8**(4), 449–462.

[4] Borisov AV, Mamaev IS [2003]. An integrability of the problem on motion of cylinder and vortex in the ideal fluid, *Reg. Chaotic Dyn.*, **8**(2), 163–166.

[5] Chyba M, Leonard NE, Sontag ED[2000]. Time-Optimal Control for Underwater Vehicles, Proc. of the IFAC Workshop on Lagrangian and Hamiltonian Methods for Nonlinear Control.

[6] Chyba M, Leonard NE, Sontag ED [2003]. Singular Trajectories in Multi-Input Time-Optimal Problems: Application to Controlled Mechanical Systems, *Journal of Dynamical and Control Systems*, **9** (1), 73-88.

[7] Eckhardt B, Aref H [1988]. Integrable and chaotic motions of four vortices II. Collision dynamics of vortex pairs, *Phil. Trans. R. Soc. Lond.*, A **326**, 655–696.

[8] Kanso E, Marsden JE, Rowley CW, Melli-Huber JB [2005]. Locomotion of articulated bodies in a perfect fluid, *J. Nonlinear Sci.*, **15**, 255–289.

[9] Kadtke JB, Novikov EA [1993]. Chaotic capture of vortices by a moving body. I. The single point vortex case, *Chaos*, **3**(4), 543–553.

[10] Li F, Aubry N[2003]. Feedback control of a flow past a cylinder via transverse motion, *Phys. Fluids*, **15**(8), 2163–2176.

[11] Marsden JE, Ratiu TS[1999]. *Introduction to Mechanics and Symmetry*, Texts in Applied Mathematics, **17**, Springer-Verlag; Second Edition, 1999.

[12] Ma Z, Shashikanth BN[2006], Dynamics and control of the system of a 2D rigid circular cylinder and point vortices, *Proceedings of the 2006 American Control Conference, Minneapolis, Minnesota, June 14–16, 2006*, 4927–4932.

[13] Marsden JE, Weinstein A [1974]. Reduction of symplectic manifolds with symmetry, *Rep. Math. Phys.*, **5**, 121–130.

[14] Milne-Thomson LM [1996]. *Theoretical Hydrodynamics* (fifth edition), Dover, New York, 1996.

[15] Newton PK [2001]. *The N-Vortex Problem: Analytical Techniques*, Applied Mathematical Sciences, **145**, Springer.

[16] Nijmeijer H, Van Der Schaft A [1990]. *Nonlinear Dynamical Control Systems*, Springer-Verlag; Third Edition, 1990.

[17] Péntek A, Kadtke JB, Pedrizzetti G[1998]. Dynamical control for capturing vortices near bluff bodies, *Phys. Rev. E*, **58**(2), 1883–1898.

[18] Pinch E [1993], *Optimal Control and the Calculus of Variations*, Oxford University Press.

[19] Pontryagin LS, Boltyanskii VG, Gamkrelidze RV, Mishchenko EF[1964]. *The Mathematical Theory of Optimal Processes (translated by D. E. Brown)*, Macmillan Company.

[20] Protas B [2004]. Linear feedback stabilization of laminar vortex shedding based on a point vortex model, *Phys. Fluids*, **16**(12), 4473–4488.

[21] Radford J[2003]. *Symmetry, Reduction and Swimming in a Perfect Fluid*, PhD Thesis, California Institute of Technology.

[22] Ramodanov SM [2002]. Motion of a circular cylinder and N point vortices in a perfect fluid , *Reg. Chaotic Dyn.*, **7**, 291–298.

[23] Spalart, P. R. [1998], Airplane Trailing Vortices, *Annual Rev. Fluid Mech.*, **30**, 107–38.

[24] Shapere A, Wilczek F [1989], Geometry of self-propulsion at low Reynolds number, *J. Fluid Mech.*, **198**, 557–585.

[25] Shashikanth BN [2005]. Poisson brackets for the dynamically interacting system of a 2-D rigid cylinder and N point vortices: The case of arbitrary smooth cylinder shapes, *Reg. Chaotic Dyn.*, **10** (1), 1-14.

[26] Shashikanth BN, Marsden JE, Burdick JW, Kelly SD [2002]. The Hamiltonian structure of a 2-D rigid circular cylinder interacting dynamically with N point vortices, *Phys. of Fluids* , **14** (3), 1214-1227.

[27] Sussmann HJ [1987]. The structure of time-optimal trajectories for single-input systems in the plane: the C^∞ nonsingular case, *SIAM J. Control and Optimization*, **25**(2), 433–465.

[28] Triantayfyllou MS, Triantayfyllou GS [1995]. An efficient swimming machine, *Scientific American*, **272**, 64–70.